

X-RAY OPTICS

PACS numbers: 52.50.Jm; 52.70.Kz
DOI: 10.1070/QE2013v043n07ABEH015128

Normal-incidence Sb/B_4C multilayer mirrors for the 80 Å $< \lambda <$ 120 Å wavelength range

E.A. Vishnyakov, D.L. Voronov, E.M. Gullikson, V.V. Kondratenko, I.A. Kopylets, M.S. Luginin, A.S. Pirozhkov, E.N. Ragozin, A.N. Shatokhin

Abstract. **Periodic and aperiodic Sb/B_4C multilayer structures have been theoretically calculated and synthesised for the first time for the application in soft X-ray optics in the 80 Å $< \lambda <$ 120 Å range. The reflection spectra of the periodic multilayer mirrors are measured using synchrotron radiation and laser plasma-generated radiation. The experimental spectra are theoretically interpreted with the inclusion of transition layers and substrate roughness. The density of antimony layers is supposedly $\rho_{(Sb)} = 6.0$ g cm^{-3}, and the thickness of transition layers (if any) in the Sb/B_4C multilayer structures does not exceed 10 Å. A peak reflectivity of 19% is attained at a wavelength of 85 Å. An aperiodic mirror optimised for maximum uniform reflectivity in the 100 – 120 Å range is tested employing the laser plasma radiation source.**

Keywords: *soft X-ray range, multilayer mirrors, antimony, aperiodic structures, normal radiation incidence.*

1. Introduction

At present, normal-incidence reflective X-ray multilayer optics are important instruments of physics research in soft X-ray (SXR) and vacuum ultraviolet (VUV) spectral ranges (λ = 30–600 Å). Periodic multilayer mirrors (MMs) are easiest to manufacture; they possess a highly selective spectral reflectivity, with the result that they are quite often employed for extracting specific lines or groups of lines from line spectra. Such mirrors based on periodic multilayer structures have found wide use in the spectroscopy of laboratory plasmas, X-ray astronomy, analytical instrument engineering, micro- and nanotechnologies (for X-ray lithography), as well as in the optics of laboratory VUV and X-ray sources (including synchrotrons and free-electron lasers).

E.A. Vishnyakov, E.N. Ragozin, A.N. Shatokhin Moscow Institute of Physics and Technology (State University), Institutskii per. 9, 141700 Dolgoprudnyi, Moscow region, Russia; P.N. Lebedev Physics Institute, Russian Academy of Sciences, Leninsky prosp. 53, 119991 Moscow, Russia; e-mail: juk301@mail.ru, enragozin@gmail.com;
D.L. Voronov, E.M. Gullikson Center for X-Ray Optics, Lawrence Berkeley National Laboratory, Berkeley, California 94720, USA;
V.V. Kondratenko, I.A. Kopylets National Technical University 'Kharkov Polytechnic Institute', ul. Frunze 21, 61002 Kharkov, Ukraine;
M.S. Luginin Moscow Institute of Physics and Technology (State University), Institutskii per. 9, 141700 Dolgoprudnyi, Moscow region, Russia;
A.S. Pirozhkov Advanced Beam Technology Division, JAEA, 8-1-7 Umemidai, Kizugawa, Kyoto 619-0215, Japan

Received 17 January 2013; revision received 26 April 2013
Kvantovaya Elektronika **43** (7) 666–673 (2013)
Translated by E.N. Ragozin

It is the practice to characterise periodic X-ray MMs by the peak reflectivity (i.e., the reflectivity at a wavelength $\lambda_0 = 2d\langle n\rangle\cos\theta$, where d is the period of the multilayer structure, $\langle n\rangle$ is the period-averaged refractive index, and θ is the angle of incidence), as well as by the shape and width of the resonance reflection peak. These optical characteristics of the MMs depend on their internal structure – on the presence of transition layers in the structure, on their thickness, density and composition, on the densities of the main MM layers (which may generally be different from the massive material densities and which affects the optical constants of the materials), as well as on the interlayer roughness and the substrate roughness. These parameters attract particular interest at the stage of synthesising new types of multilayer coatings for X-ray optics.

In the execution of experiments under laboratory conditions there also exists a demand for soft X-ray diffraction spectrometers that simultaneously possess stigmatism, a relatively large acceptance angle ($\sim 5\cdot 10^{-2}\times 5\cdot 10^{-2}$ rad), and a relatively broad operating spectral range (about an octave and over) for a resolving power $\lambda/\delta\lambda\sim 300$ and higher. We implemented such a stigmatic (imaging) spectral device using a Mo/Si normal-incidence aperiodic multilayer mirror (AMM) [1] in combination with a transmission diffraction grating.

Broadband AMMs [2] may be applied for the investigation of elementary processes involving multiply charged ions, which are performed using stigmatic (imaging) spectrographs [3–8], for the diagnostics of plasmas, including laser-produced microplasmas [9–11], for recording the high-order harmonic spectra of laser radiation and SXR pulses generated by free-electron lasers [12] or other sources, for the reflection of attosecond SXR pulses and conversion of their duration [13, 14], etc. The problem of providing the highest integral transmission coefficient after several sequential reflections in a system of several MMs with the inclusion of filter transmittances emerges, in particular, in X-ray lithography. A Mo/Si AMM optimised for maximum uniform reflectivity in the 125–250 Å range at normal radiation incidence was employed in experiments on the conversion of Ti:sapphire laser radiation ($\lambda \sim 0.8$ μm) to SXR radiation. The frequency up-conversion took place in the reflection of the radiation pulses from relativistic plasma waves driven by the multiterawatt laser radiation in a pulsed He jet (a relativistic flying mirror), and the AMM was a key element of the analysing normal-incidence spectrograph [15–17]. Optical arrangements which include MMs at only normal incidence are of especially high value in comparison with grazing-incidence arrangements, because they possess low aberrations and are suited for constructing optical images.

Table 1. Parameters of the Sb/B_4C multilayer mirrors under investigation.

Label	Number of layers	Period/Å	B_4C fraction in the period	Radius of curvature/mm	Aperture/mm
MM-1	300	43.5	0.53	plane	25×30
MM-2, MM-3	300	43.0	0.53	467	∅50.8
MM-4	600	42.9	0.53	plane	25×30
AMM 100–120	300	–	0.59 (on average)	1000	∅40.0

One of the most manufacturable pairs for the making of SXR MMs is Mo/Si, as before. However, the operating wavelength range of molybdenum–silicon mirrors is bounded below by the L absorption edge of silicon (λ = 125 Å). Attaining a relatively high reflectivity at normal incidence in a broad wavelength domain shorter that 125 Å invites the use of other material pairs. Artyukov et al. [18] analysed the optical properties of more than 1300 inorganic compounds and elements to select the material pairs which may be used as components of periodic MMs at wavelengths of 30–300 Å. The resultant data were presented in the form of tables containing information about the composition of multilayer structures, attainable reflectivities of the periodic mirrors, etc. The requirements imposed on the optical constants of the elements that make up an aperiodic structure depend on the applied optimisation criterion and, generally speaking, are different from those in the case of periodic mirrors. Nevertheless, the material pairs that yield the best results in the case of periodic MMs will, as a rule, be efficient in aperiodic structures as well.

To date, Mo/Be, Mo/Y, and La/B_4C MMs have shown the greatest promise in the spectral domain bounded above by the L absorption edge of silicon (λ = 125 Å) and below by the K absorption edge of boron (λ = 65.9 Å). In particular, Skulina et al. [19] synthesised periodic Mo/Be and Nb/Be MMs, which exhibited peak reflectivities of 69% and 58%, respectively, at a wavelength λ = 113 Å. This was a good advancement to the short-wavelength domain, but beryllium-based MMs will be inefficient at wavelengths shorter than the wavelength of K absorption edge of Be (λ = 111 Å). In a shorter-wavelength range, a reflectivity of 34% was achieved at wavelengths of 93.4 and 95.0 Å for Ru/Y [20] and Mo/Y [21] periodic mirrors, respectively. At wavelengths close to $\lambda \approx 67$ Å, in several works it has been possible to obtain reflectivities above 40% for La/B_4C MMs [22–26]. In this region, the best figures were 46.3 at λ = 66.9 Å [25] and 48.9% at λ = 66.8 Å [26]. Recently, N.N. Salashchenko's team managed to synthesise, by introducing a 3 Å thick carbon barrier layer, a $La/B_4C/C$ MM with a reflectivity of 58.6% at λ = 66.6 Å at an off-normal angle of incidence of 20° [27]. Vishnyakov et al. [28] compared different material pairs (mostly those containing yttrium) in the λ < 125 Å from the standpoint of making periodic MMs with reflections peaks at λ = 90 Å and broadband aperiodic MMs for the ranges from 80, 85, or 90 Å to 130 Å.

The present work is concerned with the theoretical and experimental investigation of MMs based on an Sb/B_4C structure; attention was first drawn to this structure in Ref. [29]. The relatively low absorption coefficient of antimony in the λ < 100 Å domain and the relatively strong departure of the real part of its refractive index from unity in the λ > 80 Å domain permits making Sb/B_4C multilayer mirrors for the 80 Å < λ < 120 Å range with reflectivities of the order of 30%–40%. All MMs under investigation were synthesised in the National Technical University 'Kharkov Polytechnic Institute' and subsequently tested using either laser-plasma or synchrotron SXR radiation sources. The spectra obtained experimentally are compared with the theoretical ones.

2. Experimental facility

An experimental investigation was made of four periodic Sb/B_4C MMs and one aperiodic MM optimised for maximum uniform reflectivity in the 100–120 Å wavelength range (Table 1). Two periodic MMs (MM-1 and MM-4) were sent to the Center for X-Ray Optics, Lawrence Berkeley National Laboratory, Berkeley, USA, for reflectivity measurements on the ALS synchrotron (Beam line 6.3.2), and the spectra of the remaining MMs were measured at the Lebedev Physics Institute (LPI) using a laser-plasma radiation source. Experiments carried out at the LPI were executed in the IKAR vacuum chamber (∅0.9×3.8 m) equipped with an oil-free pump. The residual gas pressure in the chamber was less than 10^{-4} Torr.

Located at the end flange of the vacuum chamber was a pulse-periodic Nd-doped yttrium orthoaluminate crystal laser ($Nd:YAlO_3$, 0.5 J, 6 ns, 1.08 μm). Laser plasma was produced by focusing the nanosecond laser pulses onto a tungsten target using a dense flint glass lens with a focal length f = 75 mm. The laser beam was focused onto the target to a spot with an effective area $S_{\text{eff}} \sim 10^{-5}$ cm^2; the peak intensity of laser radiation amounted to $\sim 10^{13}$ W cm^{-2} at the centre of the focal spot. The laser plasma served as a SXR source; the main experimental instrument was an imaging (stigmatic) SXR diffraction spectrograph, in which the function of the focusing element was fulfilled by the mirrors under investigation (Fig. 1). The spectrograph [30, 31] was assembled on a 0.6×3.6 m optical table in the IKAR vacuum chamber and comprised an entrance slit, an MM under investigation, a wide-aperture free-standing transmission diffraction grating, and a film holder of radius 167 mm with UF-4 X-ray photographic film, which was mounted at the prescribed distance from the grating.

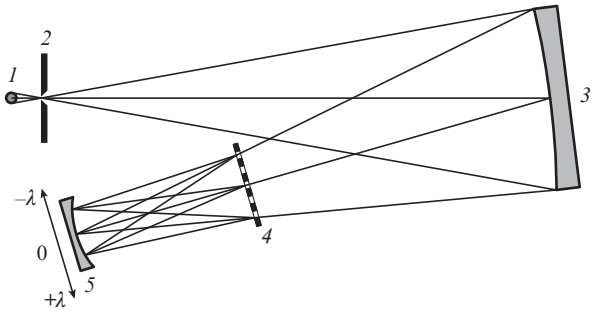

Figure 1. Schematic of the imaging (stigmatic) SXR diffraction spectrograph:
(*1*) laser plasma; (*2*) entrance slit; (*3*) MM under investigation; (*4*) transmission diffraction grating; (*5*) UF-4 photographic film holder.

Table 2. Measured optical and spectral characteristics of Sb/B_4C multilayer mirrors.

Label	Peak wavelength/Å	Incidence angle/°	Reflectivity (%)	Number of layers	Linewidth (FWHM)/Å	
					experiment	theory
MM-1	85.6	2	18.0	300	0.90	0.75
MM-2, MM-3	84.4	5	18.0	300	0.8	0.75
MM-4	84.4	2	19.6	600	0.70	0.66
AMM 100–120	100 – 120	4	2.5	300	20	20

As is commonly known [32, 33], owing to the high atomic number of tungsten the resultant plasma radiation is a quasi-continuous spectrum with an intensity smoothly varying in the 20–250 Å range. As a result, the intensity of each of the spectra recorded in our work is the product of the slowly varying spectral source intensity, the reflectivity of the MM under investigation, and the spectral sensitivity of UF-4 photographic film.

The entrance slit of the spectrograph and the UF-4 photographic film holder were located virtually on the Rowland circle of the MM under investigation, symmetrically about the mirror surface normal drawn through the point of incidence of the central ray. When measuring the spectra of the short-focus MMs, the distance between the entrance slit and the location of the zero diffraction order on the film was equal to 89 mm and in the measurement of the spectrum of the long-focus MM to 150 mm. Therefore, the radiation was reflected from the MMs at incidence angles below 0.1 rad. As a consequence, the aberrations of the configuration were small, and the spectral images of the entrance slit produced by multilayer mirrors on the photographic film emulsion were highly stigmatic.

The free-standing transmission diffraction grating was placed in the path of the beam reflected from a MM under investigation. In the measurement of the reflection spectra of the short-focus MMs we employed a 5000 line mm^{-1} gold grating with an area of 0.5 cm^2, and in the measurement of the spectrum of the long-focus MM use was made of a 1000 line mm^{-1} grating (5 cm^2). The plate scale was equal to 20 Å mm^{-1} in all experiments. In the measurement of the spectra of periodic MMs the slit width was equal to 0.6 Å and in the measurement of the AMM spectrum to 1.2 Å.

The separation of the laser plasma from the entrance slit of the spectrograph was equal to 30 mm in the case of the short-focus MMs and to 110 mm in the case of the long-focus one. Owing to the small size of the laser-plasma source (~0.05 mm), the SXR radiation emanating from each point of the entrance slit illuminated a relatively small (1–3 mm vertically) portion of the MM aperture. This permitted us to judge the multilayer coating uniformity over the MM aperture proceeding from the shape of the spectra recorded [31].

3. Experimental data and their discussion

3.1. Periodic Sb/B_4C MMs

At first the Sb/B_4C MMs under investigation were theoretically calculated and then synthesised without introducing any additional barrier layers. The optical material constants used in our calculations were borrowed from Ref. [34]. All MMs were synthesised by magnetron sputtering followed by layer-by-layer deposition on polished quartz and glass substrates (with roughness at a level of 3.5–4.0 Å) with prescribed radii of curvature. All MMs under examination bear 300 single layers (150 periods) in their multilayer structures, with the exception of MM-4 (600 layers). The geometrical and structural data on the MMs under test are collected in Table 1; the measured opticospectral characteristics are given in Table 2.

The reflection spectrum of MM-1, which contains 300 layers, is shown in Fig. 2. Its reflectivity peaks at $\lambda = 85.6$ Å at an incidence angle of 2° with respect to the MM surface normal drawn through the centre of its aperture. The measured peak reflectivity R was equal to 18.0% and the spectral width of the principal reflection peak was $\Delta\lambda_{FWHM} = 0.90$ Å.

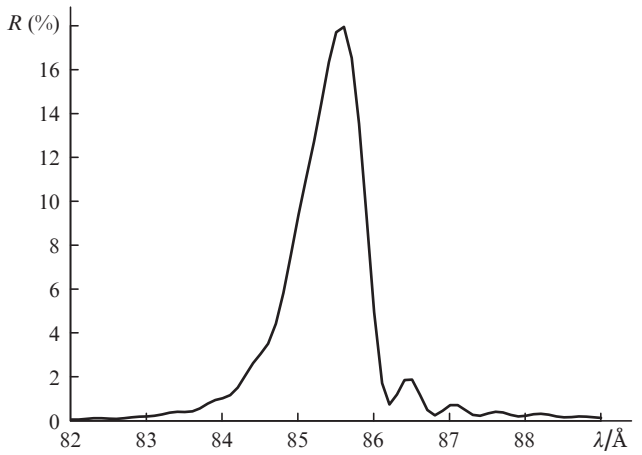

Figure 2. MM-1 reflection spectrum measured using a synchrotron radiation source.

Periodic mirrors MM-2 and MM-3 were practically the same, because they were deposited in the same deposition run at opposite ends of the carrousel with substrates, but differed only by the first layer on quartz substrates: Sb was the first layer in MM-2 and B_4C in MM-3. The reflection spectra of both mirrors were identical, but two-three months later after synthesis the MM-2 exfoliated off the substrate over almost the whole aperture (Fig. 3) due to a poorer adhesion of antimony to the quartz substrate than that of B_4C. As a result, an important technological conclusion was drawn that B_4C must be the first layer on a quartz substrate to ensure stability of Sb/B_4C MMs. The stability of MM-3 was checked a year later after its deposition, and no changes in its reflection spectrum were recorded.

The MM-2 and MM-3 reflectivity peaks fall on $\lambda = 84.4$ Å for an incidence angle of 5° from the normal drawn through the aperture centre. This corresponds to $\lambda_0 = 84.7$ Å at normal radiation incidence. Interestingly, the widths of recorded spectra $\Delta\lambda_{FWHM} = 0.8$ Å $\pm$ 0.1 Å (Fig. 4) for a theoretical width $\Delta\lambda_{FWHM} = 0.75$ Å for $N = 300$. So small a spectral width testifies to a high uniformity of the multilayer coating both over the MM aperture and with depth in the layer stack. This is

Figure 3. Exfoliation of the MM structure (the first layer on a quartz substrate is antimony).

indicative of a high quality of the new Sb/B_4C mirrors comparable to that of Mo/B_4C MMs, whose period-to-period layer thickness reproducibility is within 0.1% [35].

It is also pertinent to note that the portions of continuous spectrum, which occupy the 20–70 Å domain in the spectrum shown in Fig.4a, bear no relation to the spectra of the MMs under study. This artefact, which is present in all spectra recorded with a 5000 line mm^{-1} diffraction grating, was also

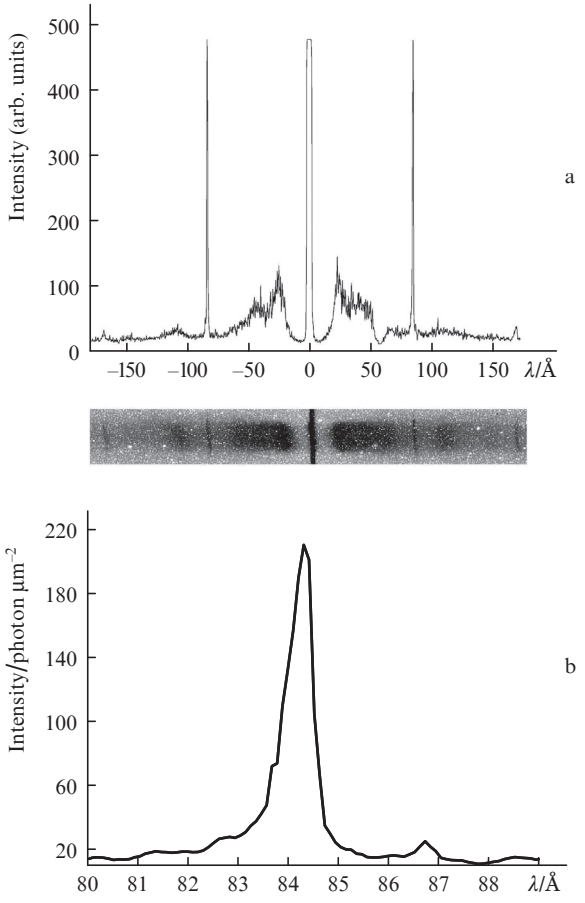

Figure 4. Panoramic reflection spectrum of periodic Sb/B_4C MMs recorded with a laser-plasma SXR source (a) and individual spectrum in the first diffraction order (b).

observed in our earlier work. This is supposedly the result of IR waves (λ = 1.5–5.0 μm) diffraction from the support structure (with a 150-μm period) of the diffraction grating. Despite the small working period of the grating, horizontally polarised electromagnetic waves may partly pass through its interbar spacings and reach the detector.

3.2. Factors responsible for MM reflectivity lowering

The calculated peak reflectivity of 300-layer Sb/B_4C MMs with $\lambda_0 \approx 85$ Å gives $R_0 = 37.8\%$. This calculation does not include the possible formation of transition layers at the interfaces between Sb and B_4C as well as the surface roughness, which will lower the real reflectivity. One more degree of freedom is the possible departure of antimony density from the tabulated one (in the crystalline state, $\rho_{Sb} = 6.7$ g cm^{-3}). It is well known that all allotropic modifications of amorphous antimony possess lower densities than crystalline antimony [36]. In the fabrication of Sb/B_4C MMs, the layers of antimony are amorphous, as shown by X-ray phase analysis. That is why it is safe to assume that in our case their density is lower than in the crystalline state. To describe our experimental data we proceeded from the assumption that the density of antimony layers in the fabricated MMs was equal to about 6.0 g cm^{-3}.

The hypothesis of the lower density of amorphous antimony is indirectly borne out by the following data. Figure 5a shows the reflectivity spectra of MM-1 and MM-4, which was measured using a synchrotron SXR source. The peak reflectivity of MM-4, which contains 600 layers, turned out to be equal to 19.6%, i.e. it increased by a factor $k = 1.09$ relative to the 300-layer MM. If the reflectivity of the 300-layer MM is taken to be unity, one can see that the saturation of calculated peak reflectivity with increasing N, the number of layers, is slower in the structures with an antimony density of 6.0 g cm^{-3} than in the structures with $\rho_{Sb} = 6.7$ g cm^{-3} (Fig. 5b). In the former case, increasing N up to 600 gives $k = 1.12$, and in the latter case only $k = 1.06$. That is, the calculation with the use of the tabulated antimony density cannot explain the rise of reflectivity from 18.0% to 19.6% with increasing N from 300 to 600. This is indication that the density of antimony in the Sb/B_4C MM supposedly lowered to 6.0 g cm^{-3} in the magnetron sputtering. The 1.09-fold rather than a 1.12-fold increase in the reflectivity of MM-4 may in turn be attributed to the development of interlayer roughness with increasing the number of layers in the Sb/B_4C structure.

The peak reflectivity R_0 calculated with neglect of substrate roughness and transition layers in the Sb/B_4C MM with $\rho_{Sb} = 6.0$ g cm^{-3} is equal to 29.7% for $N = 300$. Now when the roughness with $\sigma = 4.0$ Å is taken into account in the form of the Debye–Waller factor, we obtain $R = R_0\exp(-4\pi\sigma/\lambda)^2 = 21.0\%$. This inclusion of roughness implies that the substrate shape is reproduced without changes for all layer interfaces. If the root-mean-square roughness varies from layer to layer in the MM, the σ parameter included in the Debye–Waller factor has the meaning of the average interlayer roughness. The value $\sigma = 4.0$ Å was obtained from the simulation of small-angle scattering spectra of this multilayer structure at the CuK_α wavelength equal to 1.54 Å. The value $R = 21.0\%$ is already close to the experimentally measured one, and this allows us to assume that the main contribution to the MM reflectivity lowering is made by the lowering of antimony density to 6.0 g cm^{-3} and the interlayer roughness. We believe that further reflectivity lowering to 18% may be attributed to

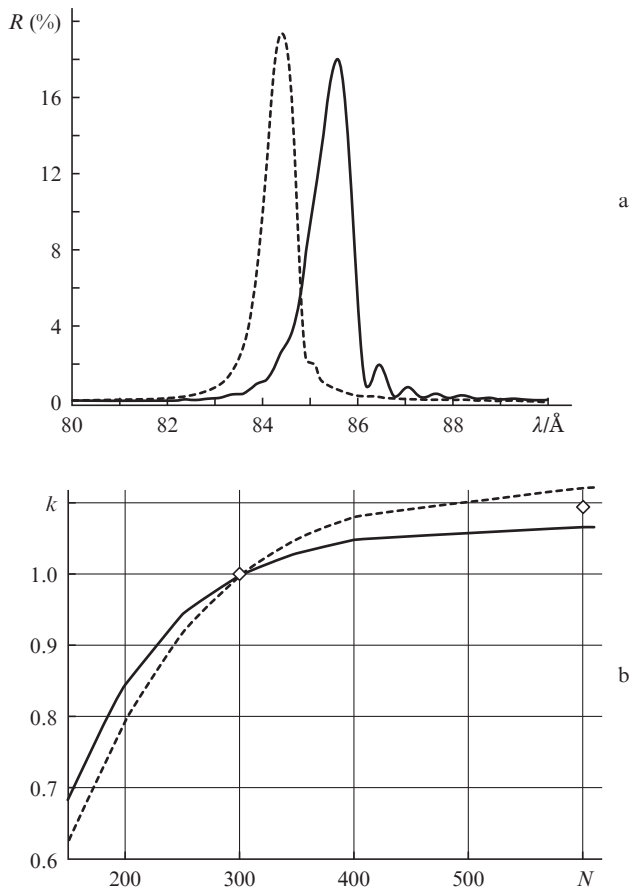

Figure 5. Reflection spectra of MM-1 (300 layers, solid curve) and MM-4 (600 layers, dashed curve) (a) and normalised reflectivity of the periodic Sb/B_4C MMs calculated as a function of the number of layers for ρ_{Sb} = 6.7 g cm^{-3} (solid curve) and 6.0 g cm^{-3} (dashed curve), diamonds represent experimental data, the coefficient R is normalised to unity for N = 300 (b).

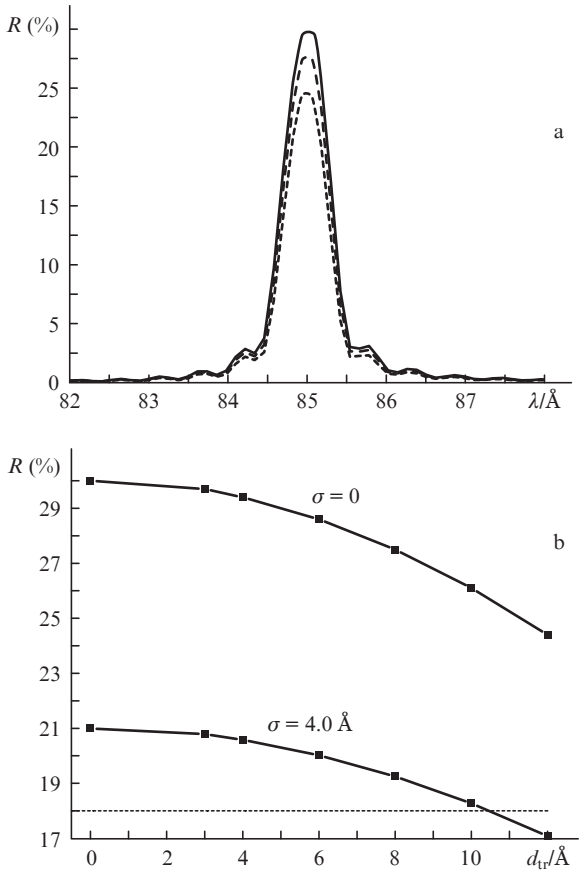

Figure 6. Reflection spectrum of Sb/B_4C periodic MMs calculated for a transition layer thickness d_{tr} = 0, 8, and 12 Å (the density of antimony used in the calculations ρ_{Sb} = 6.0 g cm^{-3}, N = 300, roughness σ = 0) (a) and dependence of the calculated MM reflectivity on the thickness of transition layers with neglect of roughness and for σ = 4.0 Å; the dashed line shows the experimentally measured reflectivity level (b).

neglected intrinsic interlayer roughness and the possible formation of transition layers in the Sb/B_4C multilayer structures.

Since the information about transition layers in Sb/B_4C structures is missing from the literature, we simulated a linear variation of the complex permittivity in the transition layers by varying their thickness [28, 29]. Increasing thickness of the transition layers in our simulations led to consistent results: the thicker are the transition layers, the lower is the peak reflectivity, this dependence being nonlinear (Fig. 6). Figure 6b shows the dependences of the peak reflectivity on the width of transition layers in the MM with ρ_{Sb} = 6.0 g cm^{-3} in two cases: with neglect of the root-mean-square roughness and with the inclusion of roughness with σ = 4.0 Å in the form of the Debye–Waller factor.

For simplicity of comparing theoretical and experimental results, all calculations displayed in Fig. 6 were performed for N = 300. The measured reflectivity of periodic MMs is represented with a dashed line in Fig. 6b. One can see: after including the lowered density of antimony layers and the rms roughness, the inclusion of transition layers gives rise to a smaller decrease in reflectivity and the thickness of transition layers (if any) does not exceed 10 Å.

So, in comparison with the ideal theoretical calculation (for ρ_{Sb} = 6.7 g cm^{-3} as well as in the absence of roughness and transition layers), with the inclusion of the lowered Sb density the MM reflectivity lowers by about a quarter, and with the inclusion of the rms interlayer roughness in the form of the Debye–Waller factor it further decreases by almost one third of the residual. Altogether, the reflectivity attainable in reality amounts to about a half of the theoretical maximum. Otherwise the Sb/B_4C MMs have exhibited a high stability, provided that B_4C was the first layer on the substrate.

3.3. Effect of transition layer thickness on the widths of spectral reflection profiles

From calculations it follows that increasing the transition layer thickness entails, apart from R lowering, a narrowing of the MM spectral reflectivity curve. This also has a simple explanation: the disappearance of abrupt interfaces between the Sb and B_4C layers is responsible for a lowering of the amplitudes of the waves reflected from each interface. On the other hand, this leads to a weaker attenuation of the incident wave and its deeper penetration into the structure. Accordingly, a greater number of MM layers are engaged and a greater number of interfering reflected rays form a narrower spectral reflectivity profile.

It is also noteworthy that the theoretical width of the MM spectral reflectivity profile calculated for 300 layers with neglect of transition layers is $\Delta\lambda_{FWHM}$ = 0.75 Å for ρ_{Sb} = 6.7 g cm^{-3} and 0.68 Å for ρ_{Sb} = 6.0 g cm^{-3}. The inclusion of

Table 3. Widths of the spectral reflectivity peaks ($\Delta\lambda_{FWHM}$/Å) of periodic MMs calculated in relation to the thickness d_{tr} of transition layers.

Accepted density of antimony/g cm^{-3}	Transition layer thickness/Å				
	N = 300				N = 600
	0	6	8	12	0
6.7	0.75 Å	0.74 Å	0.73 Å	0.70 Å	0.66 Å
6.0	0.68 Å	0.67 Å	0.66 Å	0.64 Å	0.55 Å

transition layers leads to a further narrowing of the MM spectral reflectivity profile. The calculated widths of the spectral reflectivity peaks of periodic MMs are given in Table 3 in relation to the thickness of transition layers.

3.4. Broadband aperiodic Sb/B_4C MMs

In the present work three aperiodic Sb/B_4C MMs were calculated for the 90–120 Å range. All AMMs were numerically optimised for maximum uniform reflectivity in preassigned wavelength intervals by minimising the functional $\Im_1 = \int [R(\lambda) - R_0]^2 d\lambda$ (here, R_0 is an optimisation parameter). Such mirrors, as a rule, possess a substantially higher integral reflection coefficient in comparison with any periodic mirror whose principal reflection peak lies in the same wavelength interval. For this formulation of the problem, the number of optimisation parameters is equal to the number of layers in the aperiodic structure. Periodic MMs served as the initial structures in the solution of the optimisation problem. In this case, it turned out that different initial structures may lead to virtually equipollent solutions from the standpoint of the optimisation criterion, despite the fact that their corresponding aperiodic multilayer structures may be significantly different. The structures for synthesis were selected for considerations of immunity of reflectivity spectra to small variations of individual layer thicknesses.

The reflectivity spectra calculated for the numerically optimised AMMs are given in Fig. 7. For their optimisation domains we selected the intervals 100–120 Å, 90–100 Å, and 95–105 Å. The theoretical reflectivities R averaged over their optimisation domains are equal to 5.0%, 6.0%, and 7.5%, respectively. The integral reflection coefficient $\Im_2 = \int R(\lambda) d\lambda$ in the optimisation domain was equal to ~1 Å for all AMMs. (For comparison, the calculated integral reflection coefficient of the periodic Sb/B_4C MMs with $\lambda_0 \approx 85$ Å does not exceed 0.3 Å.) The calculations were carried out for $\rho_{Sb} = 6.7$ g cm^{-3}, neglecting roughness and transition layer formation. In the optimisation we imposed a programmable limitation of 15 Å on the minimal layer thickness – for convenience of synthesis and improvement of the stability of AMM reflection spectra to deviations of the thicknesses of the basic structure layers and the formation of transition layers.

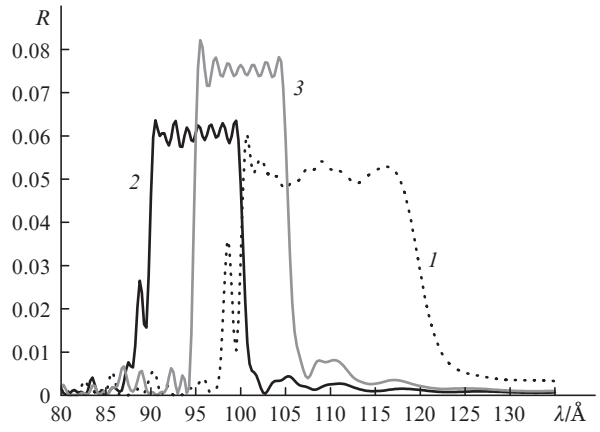

Figure 7. Calculations of Sb/B_4C AMMs with 100–120 Å (*1*), 90–100 Å (*2*), and 95–105 Å (*3*) optimisation domains (ρ_{Sb} = 6.7 g cm^{-3}).

All three AMMs have been synthesised to date, but only the AMM with the 100–120 Å optimisation domain has been studied. It was tested using a laser-plasma SXR source, the result of measurements is given in Fig. 8. Noteworthy is an excellent conformity between the spectral domain of the resultant 'plateau' and the domain of theoretical MM optimisation. Also noteworthy is a good multilayer coating uniformity over the aperture of this MM (the difference between the boundaries of optimisation domains at the opposite ends of the mirror does not exceed 1 Å). The higher long-wavelength wing in the experimental spectrum in comparison with the theoretical one is attributable to the higher luminosity of tungsten plasma in the $\lambda > 120$ Å domain than in the 50 Å < λ < 120 Å domain [37]. This is due to the fact that the experimental spectrum is the product of three functions: the plasma radiation spectrum, the MM reflectivity, and the spectral responsivity of the photographic film.

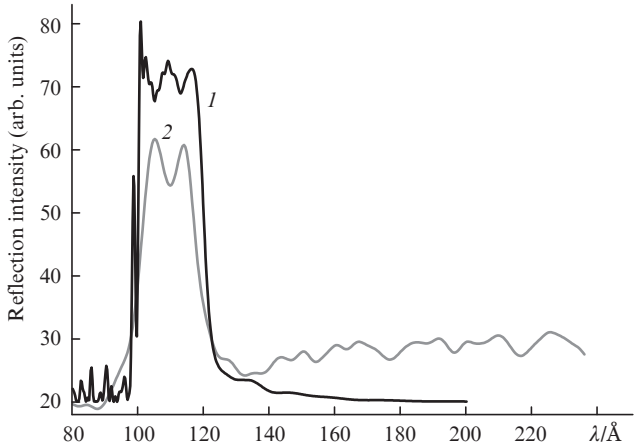

Figure 8. Theoretical (*1*) and experimental (*2*) reflection spectra of AMM-1 (100–120 Å optimisation domain).

The factors responsible for the reflectivity lowering of periodic Sb/B_4C MMs (the lowered antimony density, the rms interlayer roughness σ = 4.0 Å, and the possible existence of transition layers) manifest themselves in the same measure as in the case of AMMs. The average reflectivity in the 'plateau' of the synthesised AMM-1 is therefore likely to be equal to ~2.5%, i.e. it is two times lower than the limiting theoretical value (calculated using the tabulated antimony density ρ_{Sb} = 6.7 g cm^{-3}).

4. Conclusions

In the present work, several imaging normal-incidence multilayer mirrors based on a Sb/B_4C structure were theoretically calculated, synthesised, and tested using synchrotron and laser-plasma SXR sources. We have demonstrated the high efficiency of employing our diffraction spectrograph in combination with a broadband laser-plasma SXR source for the characterisation of normal-incidence concave MMs in the 80 Å < λ < 120 Å domain. Our measurements have demonstrated a high uniformity of the multilayer coating over the aperture and with depth, from period to period.

Periodic MMs with Sb as the first layer on a quartz substrate turned out to be unstable and exfoliated from the greater part of the aperture several months after fabrication. An important technological result was thus obtained: in the deposition of Sb/B_4C MMs, the first layer on the substrate must be a B_4C layer.

A comparison of the reflection spectra of periodic MMs with $\lambda_0 \approx 85$ Å and the ideal theoretical calculation yields a real reflectivity $R = 18.0\%$ against $R_{\text{theor}} = 37.8\%$ for $N = 300$. For all MMs under investigation, the two-fold lowering of the real peak reflectivity relative to the theoretical one can be explained by the combined effect of three factors:

1. The lowering of antimony density to 6.0 g cm^{-3} in MM layers in the magnetron sputtering (R decreases by almost 1/4).

2. The existence of interlayer roughness at a level of 4.0 Å (R additionally decreases by 1/4).

3. The possible formation of transition layers at the interfaces between Sb and B_4C.

A comparison of theoretical calculations which take into account all the above factors with the experimental data leads to a physical limitation on the maximum thickness of transition layers: even if they are formed in Sb/B_4C structures, their thickness does not exceed 10 Å.

The peak reflectivity and the spectral width of the reflectivity profile were theoretically investigated in relation to the thickness of transition layers for periodic MMs. The peak reflectivity shows a nonlinear lowering and the MM spectral reflectivity profile becomes slightly narrower with increase in transition layer thickness.

We showed that it is possible to make aperiodic Sb/B_4C MMs with an integral reflectivity ~1 Å in the 80 Å < λ < 120 Å range. One of the three synthesised AMMs was tested using a laser-plasma SXR source. We note a good correspondence between experimental data and theoretical calculations.

Acknowledgements. The authors express their appreciation to N.N. Salashchenko and P.V. Sasorov for fruitful discussions. This work was supported by the 'Fundamental Optical Spectroscopy and its Applications' Programme of the Physical Sciences Division, RAS, and the Educational-Scientific Complex of the LPI.

References

1. Kondratenko V.V., Levashov V.E., Pershin Yu.P., Pirozhkov A.S., Ragozin E.N. *Kratk. Soobshch. Fiz.*, (7), 32 (2001).
2. Kolachevskii N.N., Pirozhkov A.S., Ragozin E.N. *Kvantovaya Elektron.*, **30** (5), 428 (2000) [*Quantum Electron.*, **30** (5) 428 (2000)].
3. Ragozin E.N., Kondratenko V.V., Levashov V.E., Pershin Yu.P., Pirozhkov A.S. *Proc. SPIE Int. Soc. Opt. Eng.*, **4782**, 176 (2002).
4. Boldarev A.S., Gasilov V.A., Levashov V.E., Pershin Yu.P., Pirozhkov A.S., Pirozhkova M.S., Ragozin E.N. *Kvantovaya Elektron.*, **34** (7), 679 (2004) [*Quantum Electron.*, **34** (7), 679 (2004)].
5. Beigman I.L., Levashov V.E., Mednikov K.N., Pirozhkov A.S., Ragozin E.N., Tolstikhina I.Yu. *Kvantovaya Elektron.*, **37** (11), 1060 (2007) [*Quantum Electron.* **37** (11), 1060 (2007)].
6. Ragozin E.N., Mednikov K.N., Pertsov A.A., Pirozhkov A.S., Reva A.A., Shestov S.V., Ul'yanov A.S., Vishnyakov E.A. *Proc. SPIE Int. Soc. Opt. Eng.*, **7360**, 73600N (2009).
7. Beigman I.L., Vishnyakov E.A., Luginin M.S., Ragozin E.N., Tolstikhina I.Yu. *Kvantovaya Elektron.*, **40** (6), 545 (2010) [*Quantum Electron.*, **40** (6), 545 (2010)].
8. Beigman I.L., Vishnyakov E.A., Luginin M.S., Ragozin E.N., Tolstikhina I.Yu. *Uzhgorod Univ. Sci. Herald. Ser. Phys.*, **30**, 203 (2011).
9. Kapralov V.G., Korde R., Levashov V.E., Pirozhkov A.S., Ragozin E.N. *Kvantovaya Elektron.*, **32** (2), 149 (2002) [*Quantum Electron.*, **32** (2) 149 (2002)].
10. Levashov V.E., Mednikov K.N., Pirozhkov A.S., Ragozin E.N. *Radiat. Phys. Chem.*, **75** (11), 1819 (2006).
11. Levashov V.E., Mednikov K.N., Pirozhkov A.S., Ragozin E.N. *Kvantovaya Elektron.*, **36** (6), 549 (2006) [*Quantum Electron.*, **36** (6), 549 (2006)].
12. Louis E., Khorsand A.R., Sobierajski R., et al. *Proc. SPIE Int. Soc. Opt. Eng.*, **7361**, 73610I (2009).
13. Beigman I.L., Pirozhkov A.S., Ragozin E.N. *Pis'ma Zh. Eksp. Teor. Fiz.*, **74** (3), 167 (2001) [*JETP Lett.*, **74** (3), 149 (2001)].
14. Beigman I.L., Pirozhkov A.S., Ragozin E.N. *J. Opt. A: Pure Appl. Opt.*, **4**, 433 (2002).
15. Kando M., Pirozhkov A.S., Kawase K., et al. *Phys. Rev. Lett.*, **103** (23), 235003 (2009).
16. Pirozhkov A.S., Kando M., Esirkepov T.Zh., et al. *AIP Conf. Proc.*, **1153**, 274 (2009).
17. Pirozhkov A.S., Kando M., Esirkepov T.Zh., et al. *Proc. SPIE Int. Soc. Opt. Eng.*, **8140**, 81400A (2011).
18. Artyukov I.A., Zelentsov V.V., Krymskii K.M. *Preprint No. 14* (Moscow: Lebedev Physics Institute, Russian Academy of Sciences, 2000).
19. Skulina K.M., Alford C.S., Bionta R.M., Makowiecki D.M., Gullikson E.M., Soufli R., Kortright J.B., Underwood J.H. *Appl. Opt.*, **34** (19), 3727 (1995).
20. Barysheva M.M., Pestov A.E., Salashchenko N.N., Toropov M.N., Chkhalo N.I. *Usp. Fiz. Nauk*, **182** (7), 727 (2012).
21. Windt D.L., Donguy S., Seely J., Kjornrattanawanich B., Gullikson E.M., Walton C.C., Golub L., DeLuca E. *Proc. SPIE Int. Soc. Opt. Eng.*, **5168**, 1 (2004).
22. Platonov Yu., Gomez L., Broadway D. *Proc. SPIE Int. Soc. Opt. Eng.*, **4782**, 152 (2002).
23. Andreev S.S., Barysheva M.M., Chkhalo N.I., et al. *Nucl. Instrum. Meth. Phys. Res. A*, **603**, 80 (2009).
24. Andreev S.S., Barysheva M.M., Chkhalo N.I., et al. *Zh. Tekh. Fiz.*, **80** (8), 93 (2010).
25. Vainer Yu.A., Klyuenkov E.B., Polkovnikov V.N., Salashchenko N.N., Starikov S.D., in *'Rentgenovskaya Optika – 2012'* (Proc. of the X-Ray Optics – 2012 Conference) (Chernogolovka, 2012) p. 92.
26. Platonov Yu., Rodriguez J., Kriese M., Gullikson E., Harada T., Watanabe T., Kinoshita H. *Proc. SPIE Int. Soc. Opt. Eng.*, **8076**, 80760N (2011).
27. Chkhalo N.I., Küstner S., Polkovnikov V.N., Salashchenko N.N., Schäfers F., Starikov S.D. *Appl. Phys. Lett.*, **102**, 011602 (2013).
28. Vishnyakov E.A., Kamenets F.F., Kondratenko V.V., Luginin M.S., Panchenko A.V., Pershin Yu.P., Pirozhkov A.S., Ragozin E.N. *Kvantovaya Elektron.*, **42** (2), 143 (2012) [*Quantum Electron.*, **42** (2), 143 (2012)].
29. Vishnyakov E.A., Luginin M.S., Pirozhkov A.S., Ragozin E.N., Startsev S.A. *Kvantovaya Elektron.*, **41** (1), 75 (2011) [*Quantum Electron.*, **41** (1), 75 (2011)].
30. Zhitnik I.A., Kuzin S.V., Mitropol'skii M.M., Ragozin E.N., Slemzin V.A., Sukhanovskii V.A. *Kvantovaya Elektron.*, **20** (1), 89 (1993) [*Quantum Electron.*, **23** (1), 76 (1993)].

31. Vishnyakov E.A., Mednikov K.N., Pertsov A.A., Ragozin E.N., Reva A.A., Ul'yanov A.S., Shestov S.V. *Kvantovaya Elektron*., **39** (5), 474 (2009) [*Quantum Electron*., **39** (5), 474 (2009)].
32. Gullikson E.M., Underwood J.H., Batson P.C. *J. X-Ray Sci. Technol.*, **3**, 283 (1992).
33. Kolachevskii N.N., Pirozhkov A.S., Ragozin E.N. *Kvantovaya Elektron*., **25** (9), 843 (1998) [*Quantum Electron*., **28** (9), 821 (1998)].
34. Henke B.L., Gullikson E.M., Davis J.C. *Atom. Data Nucl. Data Tables*, **54** (2), 181 (1993); Soufli R., Gullikson E.M. *Proc. SPIE Int. Soc. Opt. Eng.*, **3113**, 222 (1997); files with refined optical scattering constants are available at <http://henke.lbl.gov/optical_constants/>.
35. Kopylets I.A., Baturin A.A., Mikhailov I.F. *Functional Mater.*, **14** (3), 392 (2007).
36. Considine G.D. *Van Nostrand's Scientific Encyclopedia* (New York: Wiley, 2008).
37. Ragozin E.N., Kolachevsky N.N., Mitropolsky M.M., Pokrovsky Yu.Yu. *Proc. SPIE Int. Soc. Opt. Eng.*, **3113**, 230 (1997).